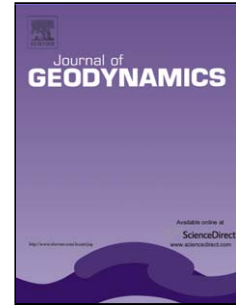


## Accepted Manuscript

Title: Simulation of free fall and resonances in the GOCE mission

Authors: Aleš Bezděk, Jaroslav Klokočník, Jan Kostecký, Rune Floberghagen, Christian Gruber



PII: S0264-3707(09)00027-1  
DOI: doi:10.1016/j.jog.2009.01.007  
Reference: GEOD 879

To appear in: *Journal of Geodynamics*

Received date: 29-10-2008  
Revised date: 27-1-2009  
Accepted date: 27-1-2009

Please cite this article as: Bezděk, A., Klokočník, J., Kostecký, J., Floberghagen, R., Gruber, C., Simulation of free fall and resonances in the GOCE mission, *Journal of Geodynamics* (2008), doi:10.1016/j.jog.2009.01.007

This is a PDF file of an unedited manuscript that has been accepted for publication. As a service to our customers we are providing this early version of the manuscript. The manuscript will undergo copyediting, typesetting, and review of the resulting proof before it is published in its final form. Please note that during the production process errors may be discovered which could affect the content, and all legal disclaimers that apply to the journal pertain.

# Simulation of free fall and resonances in the GOCE mission

Aleš Bezděk<sup>\*,a</sup>, Jaroslav Klokočník<sup>a</sup>, Jan Kostelecký<sup>b</sup>, Rune Floberghagen<sup>c</sup>,  
Christian Gruber<sup>a</sup>

<sup>a</sup>*Astronomical Institute, Academy of Sciences of the Czech Republic, Fričova 298, 251 65  
Ondřejov, Czech Republic*

<sup>b</sup>*Research Institute of Geodesy, Topography and Cartography, Ústecká 98, 250 66 Zdíby,  
Czech Republic*

<sup>c</sup>*ESA/ESRIN, Via Galileo Galilei, 00044 Frascati, Italy*

---

## Abstract

GOCE, ESA's first Earth gravity mission, is currently to be launched early in 2009 into a sun-synchronous orbit. Using the full-scale numerical propagator, we investigated the satellite's free fall from the initial injection altitude of 280 km down to the first measurement phase altitude (at 264 km). During this decay phase the satellite will pass below the 16:1 resonance (268.4 km). The effect of this resonance, together with the uncertainty in the solar activity prediction, has a distinct impact on the evolution of the orbital elements. Then, to maintain a near-constant and extremely low altitude for the measurement operational phases, the satellite will use an ion thruster to compensate for the atmospheric drag. In order to obtain the groundtrack grid dense enough for a proper sampling of the gravitational field, ESA set constraints for a minimum groundtrack repeat period. We studied suitable repeat cycles (resonant orbits) in the vicinity of 16:1 resonance; we found that

---

<sup>\*</sup>Corresponding author, tel.: +420 323620232, fax: +420 323620117.  
*Email address:* bezdek@asu.cas.cz (Aleš Bezděk)

they differ greatly in stability towards small perturbations of the satellite's mean altitude and in temporal evolution of the groundtrack coverage. The results obtained from the usual analytical treatment of orbital resonances were refined by more realistic numerical simulations. Finally, we formulated suggestions that might be useful in GOCE orbit planning.

*Key words:* GOCE, orbital propagator, orbital resonance, repeat orbit, groundtrack coverage

---

## 1 **1. Introduction**

2 The Gravity field and steady-state Ocean Circulation Explorer Mission  
3 (GOCE) is to date the most advanced gravity space mission, the first Core  
4 Earth Explorer mission of the European Space Agency's (ESA's) Living  
5 Planet programme. After a few postponements, the satellite is about to  
6 be launched in February 2009 from the Plesetsk Cosmodrome in Russia into  
7 a low altitude sun-synchronous orbit (the situation by the time when the  
8 manuscript was finalized). The satellite will carry a gradiometer, an in-  
9 strument composed of three pairs of highly sensitive microaccelerometers  
10 that measure components of the gravitational acceleration in three dimen-  
11 sions, from which the Marussi tensor of the second derivatives of the grav-  
12 itational potential is to be calculated (e.g. Hofmann-Wellenhof and Moritz,  
13 2006). The data collected are expected to significantly improve the global  
14 models of the Earth gravitational field and to provide a high-resolution  
15 map of the geoid. Apart from geodesy and positioning, a host of applica-  
16 tions are expected in geophysics, oceanography, climatology and other geo-  
17 sciences. For in-depth information about the project, refer to ESA's website,

18 <http://www.esa.int/goce/>.

19 The objective of this paper is to study two subjects connected with the  
20 GOCE mission profile: the free fall in the early orbit phase and the ground-  
21 track repeatability during the measurement operational phases. The mission  
22 is divided into several phases (see, e.g. Drinkwater et al., 2007; ESA, 1999,  
23 2004), which may be summarized as follows. The GOCE satellite will be in-  
24 jected into a dusk-dawn nearly sun-synchronous orbit to guarantee a stable  
25 and near-constant energy supply from the solar panels. *Sun-synchronicity* of  
26 the orbit means that the orientation of the satellite orbital plane is constant  
27 relative to the direction to the Sun (projected onto the equatorial plane).  
28 The *dusk-dawn* attribute says that the local time at the ascending node is  
29 18 hours, thus the orbital plane, within which the satellite circles around the  
30 Earth, will remain approximately perpendicular towards the Sun direction.  
31 From the injection altitude of 280 km, the satellite will be controlled to slowly  
32 decay down to 264 km, while the spacecraft instruments will be checked out  
33 and calibrated. The scientific requirements of the near-constant measurement  
34 altitude dictate the orbit to be circular; the sun-synchronicity condition de-  
35 termines the orbital inclination,  $96.7^\circ$ . Under such conditions, the satellite's  
36 fully sunlit trajectory will be affected by seasons of short eclipses (duration  
37 less than 10 min per orbit) and long eclipses (less than 30 min per orbit).  
38 Two, or possibly three, measurement operational phases are planned, each  
39 occupying 3–7 months, interrupted by a hibernation mode during the long  
40 eclipse seasons. The requirement for the groundtrack repeat period of GOCE  
41 to be equal or larger than two months results in the maximum separation of  
42 groundtracks less than 42 km.

## 43 2. Free fall of GOCE

44 The higher injection altitude and the subsequent free fall phase of GOCE  
45 is intended to correct potential launch injection errors in the desired orbital  
46 elements for the first measurement operational phase (MOP1); also, dur-  
47 ing the free fall phase the ion propulsion unit and the gradiometer will be  
48 checked out. In our simulation of such a fall, we tried to model all important  
49 orbital perturbative accelerations; we made use of the numerical propagator  
50 NUMINTSAT (Sec. 2.1). The aim was to get a reliable prediction of the  
51 orbital evolution and especially of the period needed for the satellite to de-  
52 scend down to the MOP1 altitude, where the drag compensation system will  
53 be activated to maintain this altitude. This prediction depends notably on  
54 the uncertainty in solar activity prediction and on the used physical charac-  
55 teristics of the spacecraft.

56 Figure 1 should be positioned here.

57 At the time of writing the manuscript, the supposed launch date was 10  
58 November 2008, 14:21 UTC. The simulated orbital evolution of the GOCE  
59 satellite, modelled as a passive freely falling body, is in Figure 1. A manifest  
60 feature of the graphs is the steady decrease in the satellite's semimajor axis  
61 (upper left panel) or equivalently mean altitude (lower right panel). By *mean*  
62 *altitude* we designate here, and henceforth, the mean semimajor axis with  
63 the Earth equatorial radius ( $R_e=6378.1363$  km) subtracted. This decrease in  
64 altitude is caused by atmospheric drag, which limits the lifetime of satellites

65 in low Earth orbits by making them finally burn up in denser layers of the  
66 atmosphere.

67 The two curves labelled as ‘*nominal*’ correspond to the nominal *satellite*  
68 *attitude*, when the side with the smallest cross-section is ahead in the direc-  
69 tion of motion. The curves labelled by ‘15° tilt’ show the orbital evolution  
70 of the satellite body, when it is slightly *tilted* relative to the velocity vec-  
71 tor. When tilted, the spacecraft’s cross-sectional area with respect to the  
72 impinging air particles is augmented, atmospheric drag is increased, and the  
73 satellite loses altitude more quickly. In Fig. 1, this is clearly visible in the  
74 evolution of semimajor axis and mean altitude.

75 The second label ‘max’ or ‘min’ (of curves in Fig. 1) refers to the maxi-  
76 mum or minimum predicted level of *solar activity*. One of the physical quan-  
77 tities determining the value of atmospheric drag is the atmospheric density,  
78 which in turn depends on the level of solar activity in UV. Solar activity in  
79 UV changes periodically over the well-known 11-year period (sunspot cycle).  
80 Unfortunately, it is not possible to predict the future time evolution of solar  
81 activity precisely enough, which may introduce a considerable amount of un-  
82 certainty in longer orbital predictions (months and more). This uncertainty  
83 due to solar activity is also evident on the hypothetical lifetime predictions  
84 for GOCE in Fig. 1, would the spacecraft be left freely falling without the  
85 activation of the drag compensation system.

86 Due to a delayed start of the new cycle of solar activity (Biesecker et al.,  
87 2008; NOAA, 2007), it seems feasible that the first measurement phase will  
88 take place below the 16:1 resonance located at 268.4 km (lower right panel  
89 of Fig. 1). A passage through an orbital resonance may cause a considerable

90 variation in the orbital elements, most visible as *quasi-secular change in*  
91 *inclination* (upper right panel of Fig. 1). Around the time of passing through  
92 the strong 16:1 resonance, the inclination may undergo negative or positive  
93 quasi-secular changes depending on the specific values of orbital elements.  
94 The exact date of 16:1 passage is apparent in Fig. 1, at day 31 for the red  
95 curve labelled ‘nominal; max’ and especially at day 45 for the green curve  
96 ‘nominal; min’, when the quasi-secular changes in inclination are significant  
97 compared to the usual periodical variations due to odd zonal harmonics. As  
98 is apparent in Fig. 1, the quasi-secular change in inclination under the 16:1  
99 resonance may occur  $\pm 15$  days relative to the exact date of passage (more  
100 on resonances in Sec. 3).

101 Our predictions were compared with predictions provided by ESA for one  
102 of the previous launch dates. Apart from solar activity, another parameter  
103 having direct influence on the atmospheric drag is the so-called *drag coeffi-*  
104 *cient*. We adopted the proposed higher value of the drag coefficient for the  
105  $15^\circ$  tilt scenarios, which enhances the rate of altitude decrease (lower right  
106 panel of Fig. 1). After this modification, we obtained comparable results  
107 for the time of the satellite descent from the injection altitude to the MOP1  
108 orbit. The graphs in Fig. 1 were obtained using the ESA values for the drag  
109 coefficient: 4.5 for the ‘nominal’ curves, 6.3 for the ‘ $15^\circ$  tilt’ ones.

### 110 2.1. *Orbital propagator NUMINTSAT*

111 For the free fall simulation of GOCE we made use of the NUMINTSAT  
112 orbital propagator, which is based on the numerical solution of the second-  
113 order differential equations of motion using the explicit Runge-Kutta method  
114 of order 8 due to Dormand and Prince (Hairer et al., 1993). The purpose of

115 NUMINTSAT is to simulate precise orbits of satellites in low Earth orbits  
116 (LEO; altitudes of 100–2000 km). In this section we want to give a brief  
117 overview of the perturbative accelerations acting on LEO satellites such as  
118 GOCE, as they are modelled by the NUMINTSAT propagator.

119 Figure 2 should be positioned here.

120 To illustrate the character of the individual perturbative accelerations, in  
121 Figure 2 we have plotted the histograms of the absolute values of accelerations  
122 encountered by GOCE. During the simulation of a one-year long orbit, we  
123 recorded the perturbative accelerations acting on the spacecraft at fixed time  
124 intervals of 20 minutes. The three panels correspond to the axes of the local  
125 reference frame, whose origin is at the spacecraft gravity centre, the *along-*  
126 *track* component lies in the direction of the satellite velocity, *cross-track* is  
127 collinear with the orbital kinetic momentum (normal to the orbital plane)  
128 and (quasi) *radial* direction completes the two preceding vectors. In order  
129 to show the strength of the individual perturbations in each component, we  
130 took the absolute values of the accelerations and divided them into magnitude  
131 classes over logarithmic scale. In this way we obtained a separate histogram  
132 (frequency distribution) for each perturbation. We do not show the actual  
133 counts on the y-axis (which is linear), as these are only formal depending on  
134 the sampling period and would add complexity to the graphs.

135 The dominant *central attraction term* due to the Earth gravity (labelled  
136 by ‘GRAV  $\mu/r$ ’ in Fig. 2) is located mainly in the radial direction because  
137 of the near circularity of GOCE’s orbit, where its value reaches  $9.02 \text{ m s}^{-2}$ .

138 In case of only central force action, the satellite's orbit would be an ellipse  
139 invariable in its shape and orientation (Keplerian ellipse). The main per-  
140 turbation to this ideal 2-body problem is the *acceleration due to oblateness*  
141 ('GRAV J2'). It is apparent in all three components, its value being roughly  
142 three orders of magnitude less than that of the central attraction. In the  
143 spherical harmonic expansion of the geopotential, the Earth's oblateness is  
144 quantified by the second zonal harmonic coefficient,  $J_2$ . The next largest  
145 perturbation, less by one to two orders of magnitude than the previous one,  
146 is caused by a composite effect of *higher degree and order geopotential terms*  
147 ('GRAV rest'), the largest of them being due to the third zonal harmonic,  $J_3$   
148 (pear-shape of the Earth).

149 Other *perturbations of gravitational origin*, of magnitudes  $10^{-8}$ – $10^{-6}$   $\text{m s}^{-2}$ ,  
150 present in all the components, are due to the attraction of the Sun and  
151 Moon ('LUNISOL'), to solid Earth tides ('SE\_TIDE') and to ocean tides  
152 ('OC\_TIDE'). The last depicted gravitational perturbation comes from the  
153 general theory of relativity ('RELATIV') and its most important action is in  
154 radial direction.

155 Now, we will describe the *nongravitational perturbations*, whose common  
156 feature is that they depend on the physical characteristics of the spacecraft,  
157 namely on its mass and shape; for that reason they are also called *surface*  
158 *forces*. *Atmospheric drag* ('DRAG') is present mainly in along-track direc-  
159 tion, where it reduces the total energy of the satellite, but it is also visible  
160 in the cross-track component. GOCE's ion thruster will counterbalance the  
161 main along-track component of drag. Finally, we consider the accelerations  
162 produced by *radiation pressures*. The largest among them is the direct so-

163 lar radiation pressure ('DSRP'), which is present in all components, when  
164 the satellite is sunlit. A special feature is a peak of almost constant size  
165 in cross-track direction brought about by the dusk-dawn character of the  
166 GOCE sun-synchronous orbit. While the reflected solar radiation ('ALB')  
167 is only faintly visible in radial component, the same magnitude range  $10^{-9}$ –  
168  $10^{-8}$   $\text{m s}^{-2}$  occupies the terrestrial infrared radiation ('IR'), which acts in  
169 radial component also at night.

### 170 3. Resonances and groundtrack coverage

171 An *orbital resonance*  $R:D$  occurs, when the satellite performs exactly  
172  $R$  nodal revolutions, while the Earth rotates  $D$  times with respect to the  
173 satellite's precessing orbital plane,  $R$  and  $D$  being coprime integers (i.e. they  
174 have no common factor other than 1). Or equivalently, a *groundtrack repeat*  
175 *orbit* has a groundtrack that repeats after an integer number  $R$  of orbital  
176 revolutions and an integer number  $D$  of nodal days, where a nodal day is the  
177 period between recurrence of the ascending node over the same Earth-fixed  
178 meridian. Because the precession of the node is much slower than the Earth's  
179 rotation rate, a nodal day differs only slightly from a solar day, and in case  
180 of a sun-synchronous orbit, they are equal. In the following, we will use the  
181 terms 'resonant orbit' and 'repeat orbit' interchangeably.

182 Resonant orbits have become noteworthy in the study of artificial satel-  
183 lites dynamics since the 1970's, e.g. to evaluate the lumped geopotential  
184 harmonic coefficients (e.g. Gooding et al., 2007; King-Hele, 1992; King-Hele  
185 and Winterbottom, 1994; Klokočník et al., 2003) or in the mission planning  
186 for Earth observing satellites, where the groundtrack repeat is a significant

187 characteristic of the orbit (Colombo, 1984; Parke and Born, 1993; Parke et al.,  
 188 1987). In the GOCE mission, the scientific requirements stipulate a gravity  
 189 field sampling at very low, constant altitude with a global and uniformly dis-  
 190 tributed dense groundtrack coverage, which leads to a repeat period equal to  
 191 or larger than 2 months (ESA, 1999). The choice of the operational altitude  
 192 is determined by the performance of the onboard ion thruster to eliminate  
 193 the air drag, and actually it seems feasible to place GOCE below 16:1 reso-  
 194 nance (Fig. 1). In this section we will discuss repeat orbits suitable for the  
 195 GOCE mission using both the linear and numerical orbit simulation.

196 Analytical treatment of orbital resonances is based on the effects of the  
 197 largest gravitational perturbation due to Earth oblateness. In terms of clas-  
 198 sical orbital elements, the second zonal term of the geopotential causes the  
 199 well-known secular changes in right ascension of the ascending node,  $\Omega$ , argu-  
 200 ment of perigee,  $\omega$ , and mean anomaly,  $M$ , (see e.g. Kaula, 1966; Zarrouati,  
 201 1987)

$$\dot{\Omega} = -\frac{3}{2}nJ_2 \left(\frac{R_e}{a}\right)^2 \cos i (1 - e^2)^{-2}, \quad (1)$$

$$\dot{\omega} = -\frac{3}{4}nJ_2 \left(\frac{R_e}{a}\right)^2 (1 - 5 \cos^2 i) (1 - e^2)^{-2}, \quad (2)$$

$$\dot{M} = n - \frac{3}{4}nJ_2 \left(\frac{R_e}{a}\right)^2 (1 - 3 \cos^2 i) (1 - e^2)^{-3/2}, \quad (3)$$

204 where  $n$  is mean motion. In terms of mean elements, where the short-period  
 205 variations over one satellite revolution are averaged out, the Earth oblateness  
 206 causes the orbital plane to precess at a constant rate  $\dot{\Omega}$ , and the perigee  
 207 to circulate at the rate given by  $\dot{\omega}$ . According to the above definition of  
 208 resonance, using the nodal period of the satellite,  $2\pi/(\dot{\omega} + \dot{M})$ , and the nodal  
 209 day,  $2\pi/(\omega_e - \dot{\Omega})$ , where  $\omega_e$  is the angular rate of the Earth, neglecting the

210 terms in  $e^2$ , we obtain (Klokočník et al., 2003)

$$n = \omega_e \frac{R}{D} \left\{ 1 - \frac{3}{2} J_2 \left( \frac{R_e}{a} \right)^2 \left( 4 \cos^2 i - \frac{R}{D} \cos i - 1 \right) \right\}. \quad (4)$$

211 For a given inclination, which in case of GOCE results from sun-synchronicity,  
 212 and for a pair of coprime integers  $R$  and  $D$ , equation (4) may be used to find  
 213 a semimajor axis for a corresponding resonant orbit. These resonant orbits  
 214 are shown in Figure 3 as red points. In accordance with the ESA's above  
 215 mentioned constraint of at least 2-month repeat period, we chose two 61-day  
 216 repeat orbits, possible candidates of the GOCE measurement phase orbits,  
 217 for more detailed analysis. For an  $R:D$  resonant orbit, after the repeat pe-  
 218 riod has been completed, the grid of groundtracks should theoretically be  
 219 homogeneous with an equatorial *node separation*

$$\Delta\lambda^{(deg)} = 360^\circ/R \quad \text{or} \quad \Delta\lambda^{(km)} = 2\pi R_e/R. \quad (5)$$

220 Thus, after 61 nodal days, the difference in density of groundtrack coverage  
 221 between the repeat orbits 977:61 and 978:61 is very small, with the equatorial  
 222 node separation of  $0.3685^\circ$  (41.02 km) and  $0.3681^\circ$  (40.98 km), respectively.  
 223 Yet, apart from the obvious 4.5-km difference in mean altitudes (Fig. 3),  
 224 the two repeat orbits do differ from, say, a practical point of view, in tem-  
 225 poral evolution of the groundtrack coverage and in stability towards small  
 226 perturbations of the mean altitude.

227 Figure 3 should be positioned here.

228 Figure 4 should be positioned here.

### 229 *3.1. Evolution of groundtrack coverage*

230 Figure 4 shows the temporal evolution with which the groundtracks cover  
231 the Earth surface for the two resonant orbits discussed above. The ground-  
232 track grid of the higher orbit 977:61 is laid down in a homogeneous way over  
233 the whole repeat period, consecutively filling up two large gaps on the equa-  
234 tor (left column of panels in Fig. 4). On the contrary, the groundtrack grid of  
235 the lower repeat orbit 978:61 is created in two phases: after the first 30 days  
236 the surface is almost homogeneously covered by a half density grid, and then,  
237 during the second 30 days, the full structure of the 978:61 homogeneous grid  
238 is completed (right column of panels in Fig. 4). In fact, after the first 30-day  
239 period, the node separation of the half-filled 978:61 grid is very close to that  
240 of the 481:30 repeat orbit, a 30-day repeat cycle with an altitude very close  
241 to that of the 978:61 orbit (Fig. 3).

### 242 *3.2. Necessary adjustment of semimajor axis to obtain groundtrack repeat*

243 The reader might have noticed a small difference in the mean altitudes of  
244 the 977:61 repeat orbit in Figures 3 and 4, and in those of the 978:61 repeat  
245 orbit. When we started to draw histograms of node separation for the two  
246 repeat orbits in order to visualize their possibly diverse characteristics, for  
247 the lower 978:61 orbit we obtained a double peaked graph of shape similar to  
248 two red bars in Fig. 5. These results were produced by analytical as well as by  
249 numerical orbit propagators (and also by ESA's simulator of GOCE's orbit).  
250 But according to the simple theoretical evaluation (Eq. 5), after the repeat

251 period is elapsed, such a histogram should produce a single peak, maybe  
252 spread around the central value  $360^\circ/R$ , but certainly not two distinctly  
253 separated peaks. In this section, we will give an explanation to this problem,  
254 and derive results, which might be useful for the GOCE measurement altitude  
255 selection.

256 Figure 5 should be positioned here.

### 257 *3.2.1. Histograms based on analytical orbit theory*

258 Let us first model and analyze the resonant orbits using a simple analyti-  
259 cal theory with only  $J_2$  perturbative term using the formulas from Tapley et  
260 al. (2004, pp. 493–497). The theory conforms to near-circular orbits, where  
261 the classical elements  $e$  and  $\omega$  fail to be mathematically well defined, by re-  
262 placing  $e$  and  $\omega$  with nonsingular elements,  $h = e \sin \omega$ ,  $k = e \cos \omega$ . It is a  
263 first-order theory in  $J_2$  based on the original Brouwer (1959) paper.

264 In Figure 5, the  $J_2$  theory was used to produce histograms of node sep-  
265 aration for the lower repeat orbit 978:61 over the completed 61-day repeat  
266 period. Each time we simulated the orbit with the specified mean altitude  
267 and collected all the longitudes of the ascending nodes; gradually these as-  
268 cending nodes reduce the gaps in longitude on the equator, as is shown in  
269 Fig. 4. Recall that the context of using the repeat orbits for GOCE is that we  
270 need no equatorial gaps larger than 42 km (or equivalently  $0.377^\circ$ ), as they  
271 are places with no direct overflight of the satellite; therefore, we are interested  
272 in the overall distribution of lengths of these gaps, after the proposed 61-day

273 repeat period is over. For this purpose we sorted the collected ascending node  
 274 longitudes and took their differences; in such a way we obtained the separa-  
 275 tions between the successive ascending nodes and could draw their histogram  
 276 for each particular simulation. To refer to the length of the equatorial gaps,  
 277 we will use the term equatorial node separation defined previously.

278 At the centre of the upper panel of Fig. 5, the blue bar is located at  
 279 the angular node separation  $\Delta\lambda \simeq 0.368^\circ$  corresponding to an exact 978:61  
 280 repeat orbit, according to Eq. (5). We obtained this single-peaked histogram  
 281 by using the mean altitude of 259.38 km, as is indicated above the bar.  
 282 Next, we reduced the mean altitude by 50 metres, and used the data from  
 283 the analytical theory to produce the histogram of node separation, which  
 284 has two distinct green bars at  $0.246^\circ$  and  $0.490^\circ$ . For the mean altitude of  
 285 259.33 km, one can find a corresponding resonant configuration in Fig. 3,  
 286 whose repeat period is 152 days: in this case, the regular groundtrack grid  
 287 is not yet finished and the histogram has two peaks (cf. the middle right  
 288 panel of Fig. 4). The histogram with the bars in cyan, and the mean altitude  
 289 259.23 km, has the larger node separation  $0.748^\circ$ . This is, in fact, the 481:30  
 290 repeat orbit, highlighted in Fig. 3. Therefore, to reduce the 61-day repeat  
 291 grid into the 30-day one, it suffices to decrease the mean altitude by only  
 292 150 metres. The unstable nature of the 978:61 repeat orbit towards only a  
 293 50-cm disturbance in mean altitude is exhibited by the histograms in the  
 294 lower panel of Fig. 5 (note the altitudes indicated above the bars).

295 By contrast, the near 61-day repeatability of orbits around the 977:61 or-  
 296 bit is preserved, even if the mean altitude is varied by  $\pm 100$  m and  $\pm 200$  m.  
 297 The histograms of such orbits are shown in Figure 6, and correspond to

298 neighbouring repeat configurations of 977:61 orbit in Fig. 3. In the case that  
299 the ion thruster should fail for a short time, an inevitable decrease in alti-  
300 tude due to air drag would follow, which for GOCE around 264-km altitude  
301 reaches 400–700 m/day. To have some safety margin, and in accordance with  
302 the planned 3–7-month duration of the measurement operational phases, a  
303 resonant configuration with a slightly higher mean altitude is worth consid-  
304 eration, e.g. the 75-day repeat orbit at 264.74 km.

305 Figure 6 should be positioned here.

306 Figure 7 should be positioned here.

307 The altitudes of resonant orbits, represented in Fig. 3, were calculated  
308 from Eq. (4). This equation was derived from secular changes in Eqs (1)–  
309 (3), the secular part of the *first approximation* of the full  $J_2$  problem, and  
310 is accurate only to first order in  $J_2$  (Klokočník et al., 2003). The mean alti-  
311 tudes calculated from Eq. (4) have an inherent uncertainty of, say, hundreds  
312 of metres. While in case of higher 977:61 orbit, the groundtrack repeatabil-  
313 ity is retained for such a deviation, for the lower 978:61 orbit much smaller  
314 departures from the exact value of the appropriate mean altitude lead to  
315 inhomogeneity in the groundtrack grids and, possibly, to shorter repeat pe-  
316 riods.

317 *3.2.2. Histograms based on numerical orbit integrator*

318 Although the simple  $J_2$  analytical theory is good enough for providing  
319 a useful approximation to orbital motion of real satellites from both theo-  
320 retical and practical aspects, when other orbital perturbations described in  
321 Sec. 2.1 are taken into account, the simulated orbits do differ from the an-  
322 alytical ones, especially during a single satellite revolution. We also take  
323 into account the lateral components of the drag, the dominant along-track  
324 drag component being balanced by the onboard ion thruster. In Figure 7, we  
325 show the histograms for several orbits near the higher 977:61 resonance. The  
326 original narrow bars from analytical theory (Fig. 6) become much wider, but  
327 still the bars are single-peaked around the theoretical 977:61 node separa-  
328 tion,  $\Delta\lambda=0.3685^\circ$ . The somewhat longer integration time of 65 days ensures  
329 that the histograms in Fig. 7 contain no bars located higher than at  $0.4^\circ$ .  
330 It is interesting that the mean altitude 263.9 km calculated from the  $J_2$   
331 analytical theory for the 977:61 resonant orbit (Fig. 6) is still valid in more  
332 realistic numerical integration for approximately 61-day repeat orbit (Fig. 7).

333

334 Let us remark here that the resonant orbits *above* the 16:1 resonance in  
335 Figure 3 are symmetrical with respect to the 16:1 mean altitude (Klokočník  
336 et al., 2008, Fig. 15), so the analysis in this section of the lower and higher  
337 example 61-day repeat orbits, closest to 16:1 altitude, is also valid ‘from  
338 above’, with the two orbits interchanged.

#### 339 4. Conclusions and suggestions for GOCE

340 In Section 2 we studied the early orbit phase of GOCE, when the satellite  
341 is let in a controlled free fall from the injection altitude of 280 km down to the  
342 first measurement phase altitude of around 264 km (Fig. 1). The anticipated  
343 passage through the strong resonance 16:1 at 268.4 km leads to changes in  
344 orbital elements, especially to the quasi-secular drift in inclination, which  
345 may reach  $\pm 0.03^\circ$ . Recall that using the onboard ion thruster GOCE can  
346 only adjust its semimajor axis. As inclination and semimajor axis are key  
347 parameters in both sun-synchronicity and repeatability conditions, and after  
348 the passage through 16:1 resonance the inclination will be perturbed and  
349 may take some value differing from  $96.7^\circ$ , it would be advisable to re-adjust  
350 the semimajor axis according to the actually measured values of inclination  
351 to ensure at best the orbit requirements, *after* the satellite will have passed  
352 through 16:1 resonance.

353 In Section 3, we analyzed some properties of near-repeating orbits suit-  
354 able for GOCE measurement operational phases. We selected two 61-day  
355 repeat orbits as examples, the higher 977:61 orbit at 263.9 km, and the lower  
356 978:61 orbit at 259.4 km (Fig. 3). After the repeat period of 61 days is com-  
357 pleted, the groundtrack grids of both example orbits should theoretically be  
358 almost the same, with homogeneous coverage and equatorial node separation  
359 of 41 km. We show in Figure 4 that while the groundtrack grid pertaining to  
360 the higher 977:61 orbit covers the Earth's surface consecutively, that of the  
361 lower 978:61 orbit is laid down in two 30-day phases, each time a shifted half-  
362 density grid is created. Varying the mean altitudes by small steps around  
363 the exact resonance value for the two example orbits, we found their rather

364 different behaviour in theoretical as well as practical aspects. The double-  
365 peaked shape of the histograms of node separation for orbits near the lower  
366 978:61 repeat orbit (Fig. 5) show clearly that the orbit loses the exact re-  
367 peatability character already with a 50-cm variation (Fig. 5, lower panel)  
368 and that a 150-metre decrease in mean altitude reduces the repeat period  
369 from 61 days to 30 days (upper panel). To the contrary, the histograms  
370 of orbits neighbouring the higher 977:61 repeat orbit are single-peaked and,  
371 therefore, these orbits retain their repeating character even if the mean al-  
372 titude is varied by  $\pm 200$  m (Fig. 6). The conservation of the repeatability  
373 character for the higher 977:61 orbit towards a few hundred metres variations  
374 were tested using the full numerical integration, the narrow histogram peaks  
375 obtained from the analytical computations became broadened (Fig. 7). We  
376 would, therefore, suggest that, from the point of view of repeatability conser-  
377 vation towards the mean altitude variations, the repeat orbit for the GOCE  
378 measurement operational phases be located on the upper branch of resonant  
379 orbits in Fig. 3, which contains the 977:61 configuration. Due to variations  
380 in semimajor axis, or to a possible short-term failure of the onboard ion  
381 thruster, an orbit of slightly higher mean altitude might be advisable, which  
382 would have, say, 75-day repeat period and an altitude of 264–265 km.

383 Let us, finally, note one practical lesson learnt from the simulations of  
384 Section 3. A simple way for finding the value of mean altitude that ensures  
385 the near repeatability condition to be fulfilled, when one is interested in the  
386 modelling of *real orbital conditions* using the full numerical integrator, is  
387 to use the given (or measured) values of osculating elements, to make the  
388 integrator predict orbits for an appropriate range of semimajor axis values,

389 and to draw the histograms of node separation, which show the repeatability  
390 character of the orbit considered (like Fig. 7). The ion thruster may then be  
391 used to adjust the semimajor axis to the chosen optimum value.

## 392 **5. Acknowledgements**

393 The authors are grateful to an anonymous reviewer for detailed comments  
394 and helpful suggestions. This work was supported by the ESA/PECS grant  
395 C 98056.

## 396 **References**

- 397 Biesecker, D. A., and the Solar Cycle 24 Prediction Panel, 2008. Solar Cycle  
398 24 Prediction Panel Update. Space Weather Workshop, 29 April–2 May,  
399 Boulder, Colorado, USA.
- 400 Brouwer, D., 1959. Solution of the problem of artificial satellite theory with-  
401 out drag. *Astron. J.* 64, 378–397.
- 402 Colombo, O. L., 1984. Altimetry, orbits and tides. NASA Tech. Memo.,  
403 NASA TM-86180.
- 404 Drinkwater, M. R., Haagmans, R., Muzi, D., Popescu, A., Floberghagen, R.,  
405 Kern, M., Fehring, M., 2007. Proceedings of 3rd International GOCE  
406 User Workshop, 6–8 November, Frascati, Italy, ESA SP-627.
- 407 ESA, 1999. Gravity Field and Steady-State Ocean Circulation Mission, re-  
408 port for mission selection of the four candidate Earth Explorer missions.  
409 ESA SP-1233(1).

- 410 ESA, 2004. GOCE Ground Segment Concept and Architecture, GO-TN-  
411 ESA-GS-0017.
- 412 Gooding, R. H., Wagner, C. A., Klokočník, J., Kostelecký, J., Gruber, C.,  
413 2007. CHAMP and GRACE resonances, and the gravity field of the Earth.  
414 *Advances in Space Research* 39, 1604–1611.
- 415 Hairer, E., Nørsett, S. P., Wanner, G., 1993. Solving ordinary differential  
416 equations I. Nonstiff problems. Springer.
- 417 Hofmann-Wellenhof, B., Moritz, H., 2006. *Physical Geodesy. Physical*  
418 *Geodesy*. ISBN 3-211-33544-7, Springer, Berlin.
- 419 Kaula, W. M., 1966. *Theory of satellite geodesy. Applications of satellites to*  
420 *geodesy*. Waltham, Mass.: Blaisdell.
- 421 King-Hele, D. G., 1992. *A Tapestry of Orbits*, ISBN 052139323X, Cambridge  
422 University Press.
- 423 King-Hele, D. G., Winterbottom, A. N., 1994. Comparison of geopotential  
424 harmonics in comprehensive models with those derived from satellite res-  
425 onance, 1972-1993. *Planet. Sp. Sci.* 42, 359–365.
- 426 Klokočník, J., Kostelecký, J., Gooding, R. H., 2003. On fine orbit selection for  
427 particular geodetic and oceanographic missions involving passage through  
428 resonances. *Journal of Geodesy* 77, 30–40.
- 429 Klokočník, J., Wagner, C. A., Kostelecký, J., Bezděk, A., Novák, P.,  
430 McAdoo, D., 2008. Variations in the accuracy of gravity recovery due

- 431 to ground track variability: GRACE, CHAMP, and GOCE. *Journal of*  
432 *Geodesy*, 22–32.
- 433 NOAA, 2007. Next solar storm cycle will start late. Press release, April 25,  
434 <http://www.swpc.noaa.gov/SolarCycle/SC24/PressRelease.html>.
- 435 Parke, M. E., Born, G., 1993. The effects of altimeter sampling characteris-  
436 tics: Some Geosat examples. Naval Research Lab. Report.
- 437 Parke, M. E., Stewart, R. H., Farless, D. L., Cartwright, D. E., 1987. On the  
438 choice of orbits for an altimetric satellite to study ocean circulation and  
439 tides. *J. Geophys. Res.* 92, 11693–11708.
- 440 Tapley, B. D., Schutz, B. E., Born, G. H., 2004. *Statistical Orbit Determi-*  
441 *nation*. Elsevier Academic Press.
- 442 Zarrouati, O., 1987. *Trajectoires Spatiales*. Cepaudes-Editions, Toulouse.

443 **Figure captions**

Figure 1: Mean orbital elements calculated by NUMINTSAT (GOCE free-fall simulation; start: 10 Nov 2008).

Figure 2: Histograms of gravitational and nongravitational accelerations in the local reference frame components (simulation for GOCE, 10/2008–10/2009, altitude 263.9 km).

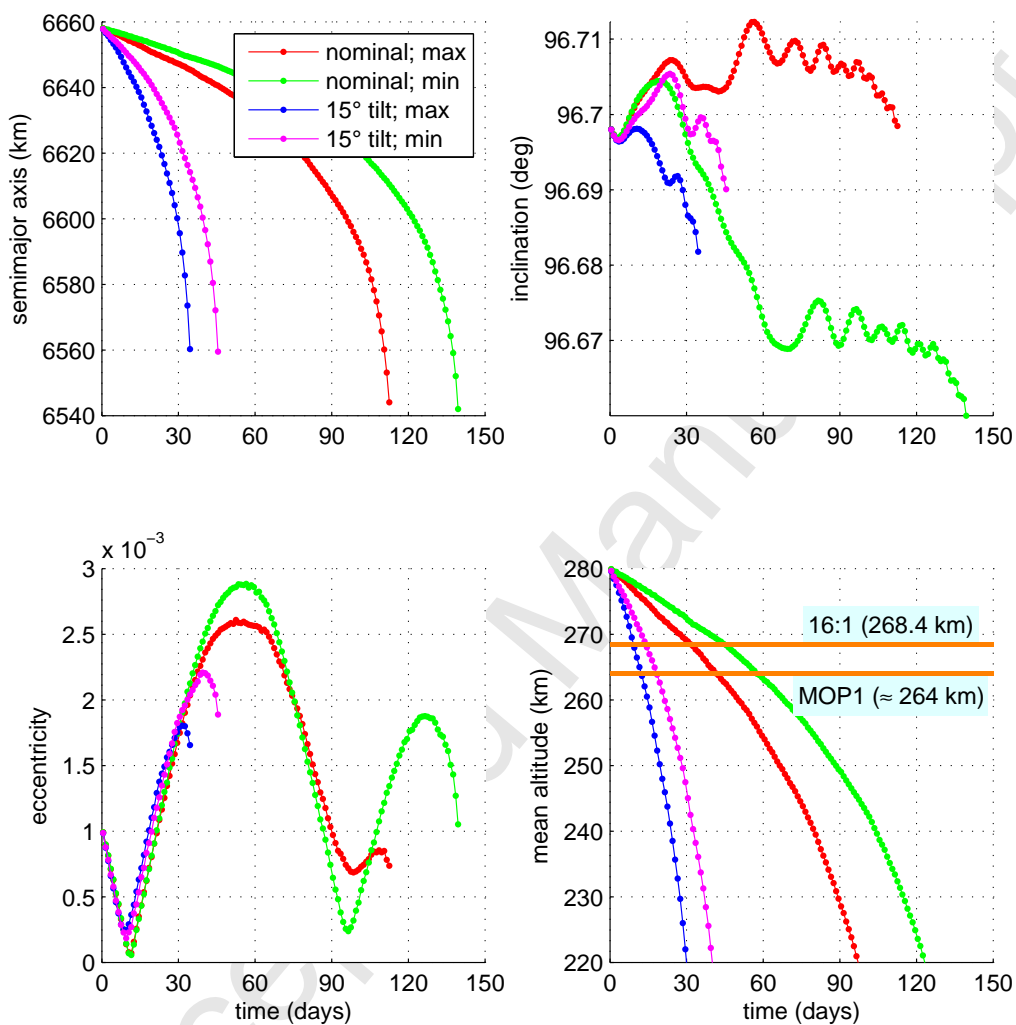
Figure 3: Orbital resonances predicted for GOCE (inclination  $96.7^\circ$ ).

Figure 4: Evolution of groundtrack grid for resonant orbits 977:61 and 978:61. Only a subsection of the ascending parts of the orbit is drawn.

Figure 5: Histograms of node separation for orbits near the 978:61 resonance as function of the mean altitude (which is indicated above the bars). The data were calculated using the  $J_2$  analytical theory.

Figure 6: Histogram of node separation for orbits near the 977:61 resonance. The data were calculated using the  $J_2$  analytical theory.

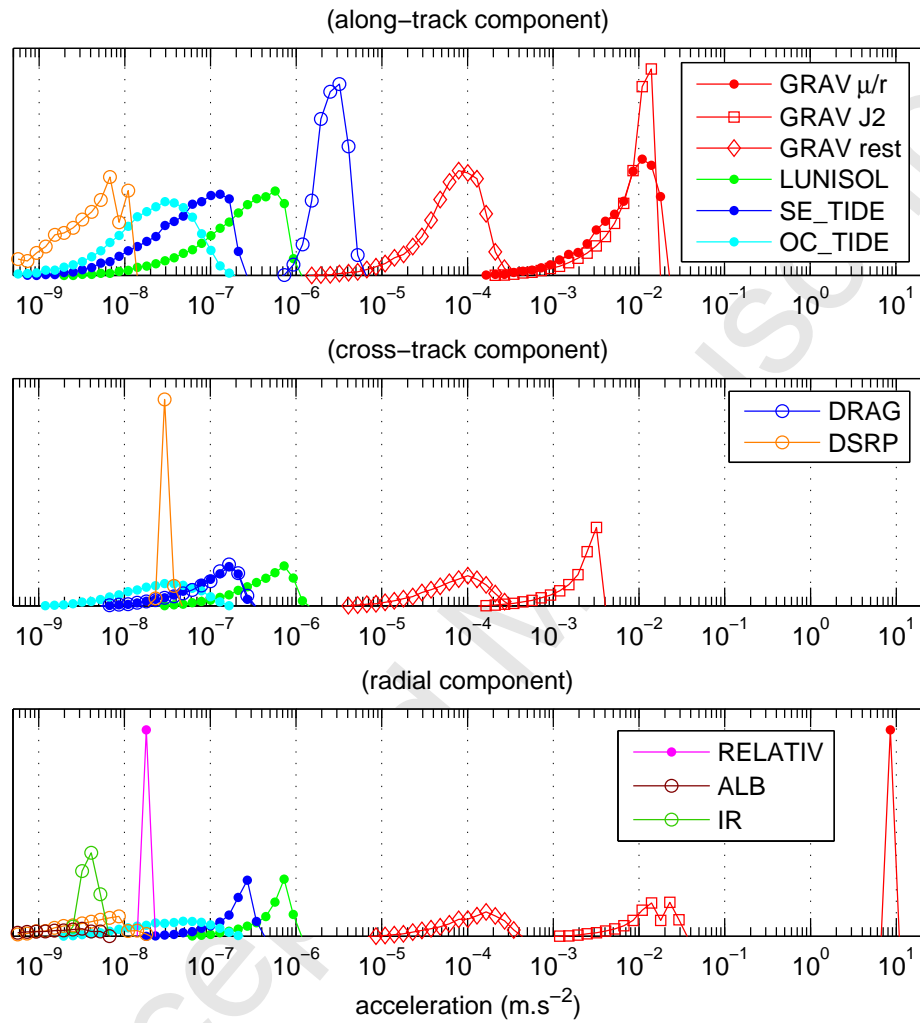
Figure 7: Histogram of node separation for orbits near the 977:61 resonance. The simulated data from 65 days using the EGM 2008 geopotential up to degree/order 50 and all orbital perturbations depicted in Fig. 2.



444

445

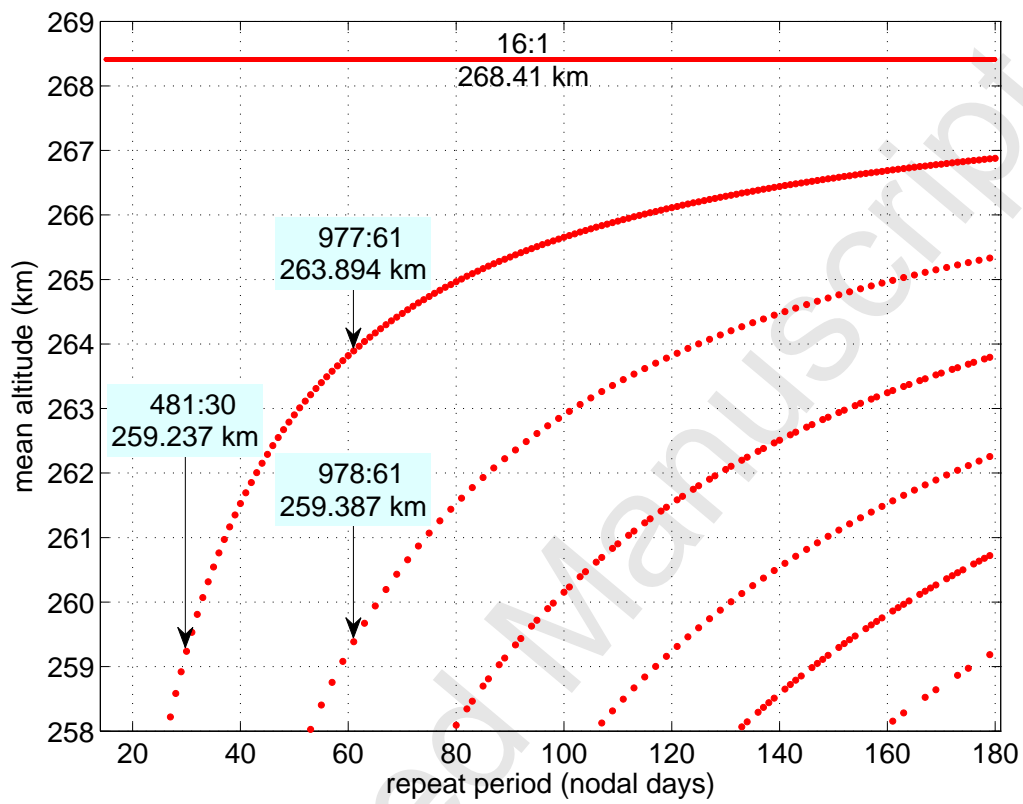
Figure 1



446

447

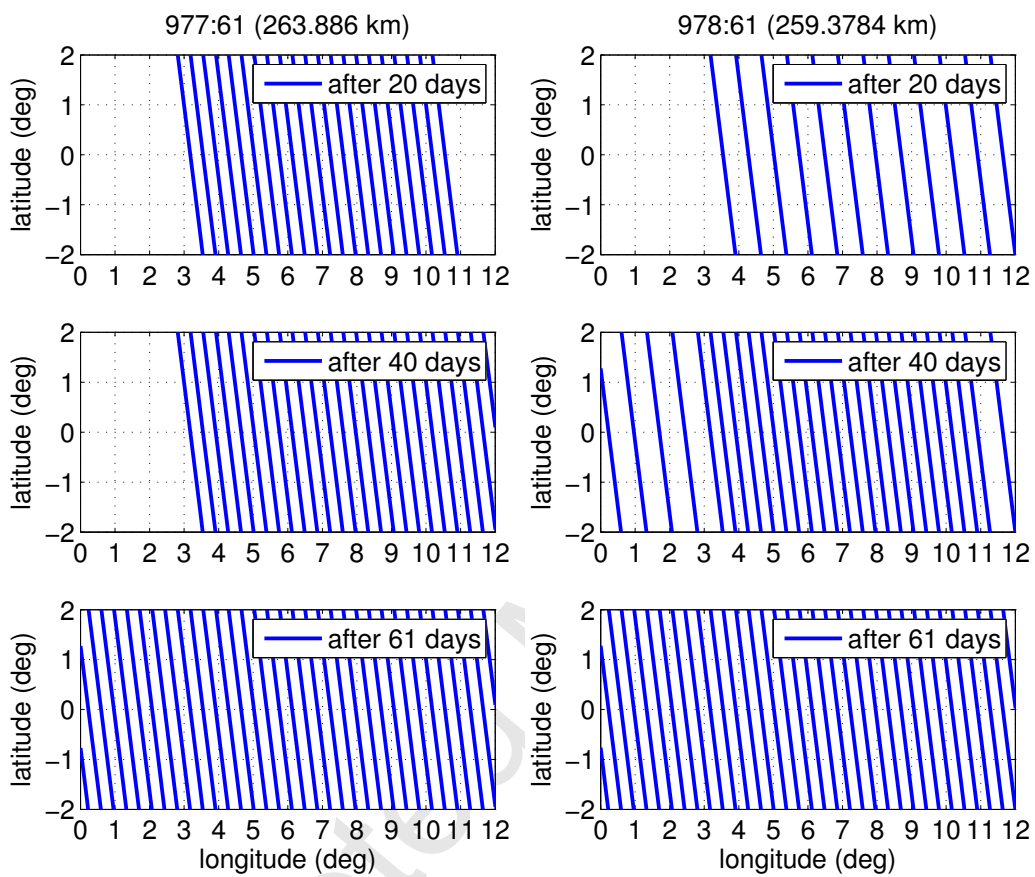
Figure 2



448

449

Figure 3



450

451

Figure 4

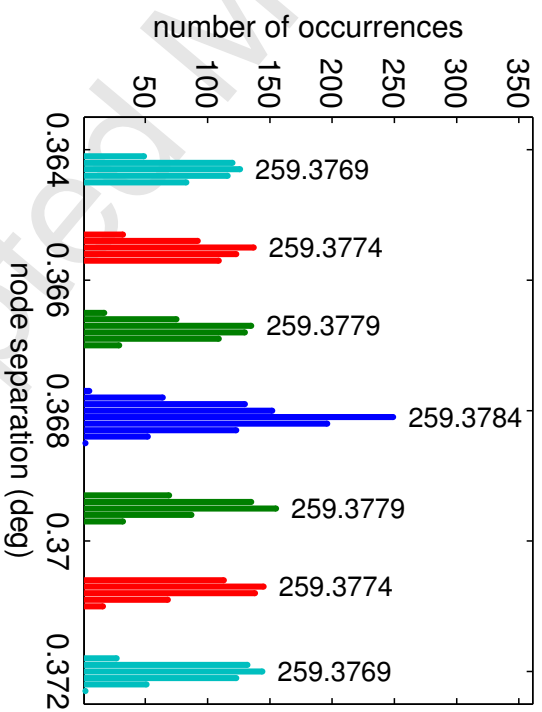
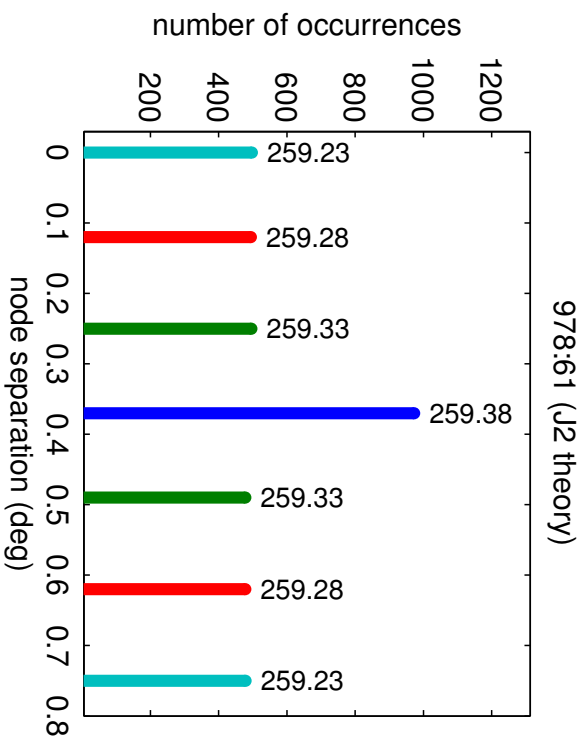
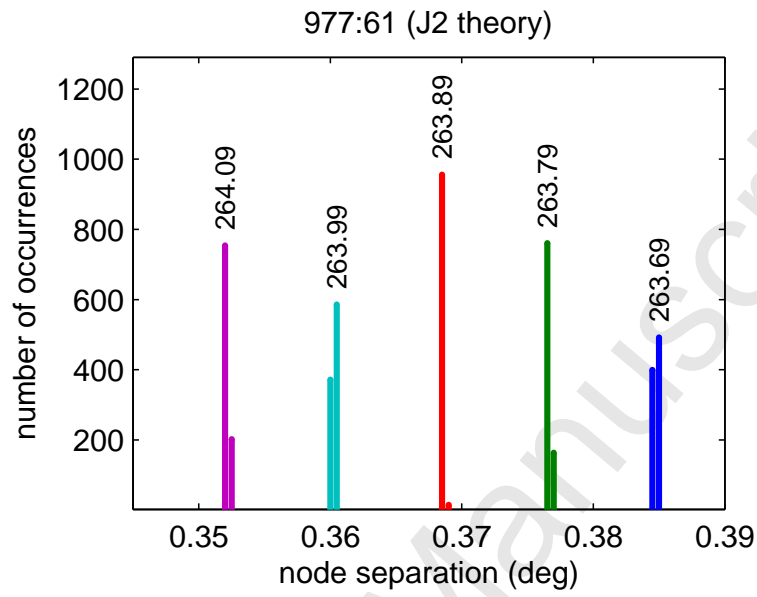


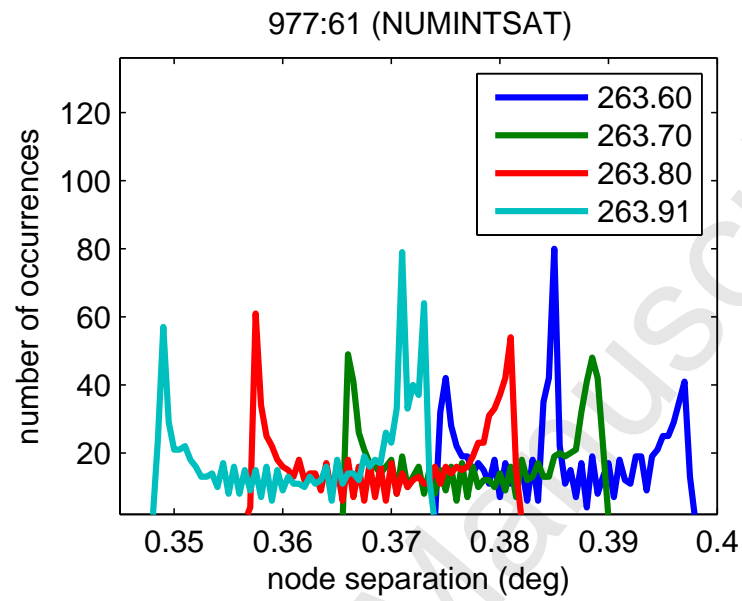
Figure 5



454

455

Figure 6



456

457

Figure 7